ONE-DIMENSIONAL CONVECTIVE AND CONDUCTIVE GEOTHERMAL HEAT FLOW

J. C. Martin, R. E. Wegner and F. J. Kelsey
Chevron Oil Field Research Co.
P.O. Box 446, LaHabra, Ca. 90631

A number of research workers have investigated two- and three-dimensional natural convective heat flow in porous media containing a single-phase fluid[1,2]. Results indicate that convective heat flow in geothermal reservoirs can be high with low geothermal gradients within the convection cells.

Single-phase convection can occur only in two or three dimensions; however, it is evident that steam and hot water sometimes exist simultaneously in geothermal areas. The large difference in density between steam and hot water provides a driving force that tends to segregate the two phases, making countercurrent vertical one-dimensional fluid flow theoretically possible.

This paper presents the results of a study of one-dimensional, vertical, two phase, steady-state, geothermal fluid and heat flow. Steam is assumed to be generated at depth by heat conducted from below. The steam flows upward and an equal mass of hot water flows downward within the geothermal reservoir. At the top of the geothermal reservoir the steam condenses into hot water which then flows downward. Above the reservoir the heat flow is again only conductive.

A method of calculating one-dimensional, combined convective and conductive heat flow is presented with calculated examples. The object of the investigation was to understand the one-dimensional convective heat flow that may occur where conditions have been stable long enough for the flow to approach steady-state. Results presented herein apply to unfractured porous media. Similar results should apply to fractured reservoirs and permeable fault zones.

The water is assumed sufficiently fresh that the effects of dissolved solids can be neglected. The surface temperature and heat flow rate are assumed to be known. Capillary pressure and steam and hot water relative permeabilities are used in the analysis; however, the effects of capillary pressure were neglected in the example calculations. The analysis allows the thermal conductivity to vary with temperature and steam or hot water saturation; however, for simplicity a constant value was used in the calculations.

DISCUSSION

Appendix A gives the equations of heat and fluid flow, and the derivation of the two equations below. These can be solved simultaneously to obtain the steam saturation and the temperature-pressure point on the boiling curve as functions of depth.

$$AG_v + BG_d = 1 \tag{1}$$

$$\frac{dp}{dz} = \frac{g\rho_w{}^2\lambda_w + g\rho_s{}^2\lambda_s}{\rho_w\lambda_w + \rho_s\lambda_s} \tag{2}$$

Symbols are defined in Appendix B. If one dimensional, two phase convective flow is possible, equation 1 can be solved for the steam saturation. This result can be used with equation 2 to calculate the pressure gradient.

In equation 1, AG_v is the fractional convective heat flow; BG_d is the fractional conductive heat flow. For a given problem coefficients A and B are constants, and G_v and G_d determine the variations in the convective and conductive heat flow. Both G_v and G_d are functions of the relative permeabilities, the fluid saturations, the temperature-pressure point on the boiling curve, and the fluid properties. In addition, G_v is a function of the steam-hot water enthalpy difference and G_d is a function of the variations in thermal conductivity.

Figure 1 presents the two sets of steam-hot water relative permeability curves used in the calculations. Type II relative permeability curves were included because recent experimental results reported by Brigham[3] indicate high immobile water saturations. Figure 2 presents the variation of G_v with steam saturation for various pressures for Type I relative permeability curves. This curve is "bell" shaped because the mass flow of steam upward must equal the mass flow of water downward. The relative permeability to steam controls the shape of the curve at low values of steam saturations, S_s, and the relative permeability to hot water controls the shape at high values of S_s.

Figure 2 indicates that the temperature-pressure point on the boiling curve also has a strong effect on G_v. At lower temperature-pressure values the relatively high water viscosity depresses the curve, causing the maximum G_v to occur at higher steam saturations. At high temperature-pressure values, the curves are depressed by smaller differences in densities and enthalpies. At critical conditions these differences are zero, hence one-dimensional convection cannot exist.

Figure 3 presents G_d versus S_s for various pressures for Type I relative permeability curves. The sharp decline in G_d at higher S_s results from the low density of steam as compared to that of hot water. The high G_d at low pressures results from the steep slope of the boiling curve, $\psi(p)$.

Figure 4 presents the variation of AG_v, BG_d, and $AG_v + BG_d$ with S_s for Type I relative permeability curves, $T = 435^{\circ}F$, $P = 362$ psia, $k = .010$ darcys, $Kh = 40$ Btu/day-ft-$^{\circ}F$, and $u_h = -6$ Btu/day-ft^2. To satisfy equation 1, $AG_v + BG_d$ must equal 1. Two values of S_s satisfy this condition (Figure 4). The lower steam saturation, S_s1, is associated with conditions approximating a hot water column through which steam is migrating upward and the hot water downward. For a wide range of conditions, the pressure gradient approximates that of hot water, causing a corresponding rapid increase in temperature and pressure with depth. This relatively large temperature gradient can cause significant conductive heat flow.

The higher steam saturation, S_{s2}, is associated with conditions approximating a steam column with a small amount of mobile hot water. In this case there is a wide range of conditions in which the pressure gradient is very low, approximating that of steam. This very low increase in pressure and temperature with depth results in low conductive heat flow.

At a steam-hot water interface or contact, the high steam saturation, S_{s2}, exists above the interface, and the low steam saturation, S_{s1}, exists below it. If capillarity is included, the interface becomes a steam-hot water transition zone, in which capillarity determines the saturation distribution.

Figure 5 presents the results of a series of calculations in which an impermeable zone exists to a depth of 2500 feet, from which a permeable (10 md) geothermal reservoir extends to a depth of 10,000 feet. Below this there is another impermeable zone. The surface temperature is chosen to be $60^{\circ}F$, and the conditions at the top of the reservoir are those used in Figure 4. Both impermeable zones were assigned a thermal conductivity of 40 Btu/day-ft-$^{\circ}F$. Figure 5 presents the variations in temperature, pressure, steam saturation and conductive heat flow with depth for both Type I and Type II relative permeability curves. Only the steam saturation for the S_{s2} solution changes significantly with relative permeability. As mentioned previously, the S_{s1} solution approximates conditions in a hot water column, in which the pressure increases with depth according to a hot water gradient. This requires a corresponding increase in temperature to maintain boiling conditions. The increase in temperature results in significant conductive heat flow. The S_{s2} solution approximates conditions in a steam column, and the low steam density results in low temperature and pressure gradients, and very small conductive heat flow.

Figure 6 presents the results of calculations similar to those of Figure 5, except there is a steam-hot water interface at -10,000 feet. The S_{s2} solution applies from -2500 feet to -10,000 feet and the S_{s1} solution applies below -10,000 feet. Here again only the steam saturation for the S_{s2} solution changes significantly with relative permeabilities. Steam generated at the bottom of the reservoir migrates upward until it reaches the top where it condenses. Throughout the column sufficient phase transfer takes place between the steam and hot water to maintain steady-state heat and fluid flow.

Figure 7 presents an example with and without a steam-hot water interface at 5,000 feet. Both the S_s1 and S_s2 solutions are shown below this depth. The S_s1 solution approaches critical conditions at -15,550 feet. The calculations indicate that convective heat flow does not approach zero to within a few degrees of the critical temperature. This occurs even though the driving force (the difference in density) and the enthalpy difference both approach zero as critical conditions are approached. This seemingly inconsistent result is caused by the very low slopes of the density and enthalpy differences as the critical conditions are approached (Figure 8). Calculations indicate that below the point where critical conditions are reached a single phase exists which is above critical conditions. There is a reduction in the pressure gradient as illustrated in Figure 7 and the heat flow is purely conductive.

Results of calculations not presented herein indicate that it is possible to encounter conditions below the critical beyond which only superheated steam exists. Both S_{s1} and S_{s2} solutions encounter these conditions. They occur at the maximum value of the $AG_v + BG_d$ curve.

Figure 4 indicates that the $AG_v + BG_d$ curve may extend to much lower values in the high S_s range than for the low range. In some cases where A and B are sufficiently large, only S_{s2} solutions exist. Since A and B vary inversely with u_h, these conditions are more likely to occur for low u_h values. Calculations indicate that this type of solution may be valid and have significant convective heat flow over many thousands of feet for low permeabilities even less than 0.1 md. It is conceivable that this type of fluid and heat flow may be taking place at great depths in tectonically active regions where permeability may be being maintained by fracturing. The increased heat flow could be responsible for areas of increased heat flow near faults.

The lower limit of permeability for which physically meaningful solutions can be obtained has not been determined. Numerical solutions have been obtained for extremely small values of permeability and fractional convective heat flow, AG_v. In these solutions the S_s varies in such a manner that both the fluid pressure gradient and the boiling curve conditions are

satisfied. These steady-state solutions assume that all transients have died out. Thus, the lower permeability limit depends on the conditions of the problem and on the time required to reach steady-state.

The results presented in Figures 4-8 are for a total heat flow of -6 Btu/ft^2-day and a reservoir permeability of 10 md. Other calculated results indicate that the overall fluid and heat flow is relatively insensitive to a wide range of conditions.

Conclusions

1. Combined one-dimensional, vertical, convective and conductive heat flow is theoretically possible in geothermal reservoirs. Calculations indicate that this can occur over depths ranging from the surface to below 20,000 feet.

2. In many cases two fluid saturations satisfy the same heat flow rate. One is a high hot water saturation in which hot water is the principal mobile phase. The pressure gradient is approximately that of the hot water. The other fluid saturation is a high steam saturation in which steam is the principal mobile phase, and the pressure gradient is approximately that of steam. Only the steam saturation changed significantly with relative permeability for the two sets of relative permeability curves investigated.

3. For permeabilities greater than 1 md and for high steam saturations, the convective fraction of the heat flow is generally many times the conductive fraction. For high hot water saturations the two fractions are often of comparable magnitudes.

4. Convective heat flows involving high steam saturations can extend to considerably greater depths than those involving high water saturations.

REFERENCES

1. Combarnous, M. A. and Bareis, S. A., "Hydrothermal Convection in Saturated Porous Media", Advances in Hydroscience, Vol. 10, Ven Te Chow Editor, Academic Press, 1975, pp. 231-307.

2. Wooding, R. A., "Methods of Solution of the Equations for Convection in Porous Media, with Geothermal Applications", Workshop on Geothermal Reservoir Engineering, December 15-17, 1975, P. Kruger and H. J. Ramey, Jr., Editors, SGP-TR-12 Stanford Geothermal Program, Stanford University.

3. Brigham, W., "Recent Flow and Equilibria Experiments in the Stanford Geothermal Program", Paper presented at the second Workshop on Geothermal Reservoir Engineering, Stanford University. December 1-3, 1976.

APPENDIX A

The equations used in the numerical solution are derived in this appendix. All equations written in a consistent set of units, and the symbols are defined in Appendix B.

The basic equations are:

Darcy's law for hot water $$u_w = -\lambda_w \left(\frac{\partial p_w}{\partial z} - g\rho_w\right) \qquad (A\text{-}1)$$

Darcy's law for steam $$u_s = -\lambda_s \left(\frac{\partial p_s}{\partial z} - g\rho_s\right) \qquad (A\text{-}2)$$

Continuity equation for mass $$\frac{\partial}{\partial z}(\rho_w u_w + \rho_s u_s) = -\frac{\partial}{\partial t}[\phi(\rho_w S_w + \rho_s S_s)] \qquad (A\text{-}3)$$

Saturations $$S_w + S_s = 1 \qquad (A\text{-}4)$$

Continuity equation for heat $$\frac{\partial u_h}{\partial z} = -\phi \frac{\partial}{\partial t}\left[\rho_w h_w S_w + \rho_s h_s S_s + \left(\frac{1-\phi}{\phi}\right)\rho_r c_r T\right] \qquad (A\text{-}5)$$

Heat flow $$u_h = \rho_w h_w u_w + \rho_s h_s u_s - k_h \frac{\partial T}{\partial z} \qquad (A\text{-}6)$$

Capillary pressure $$p_s - p_w = P_c(S_s, T) \qquad (A\text{-}7)$$

Boiling curve $$T = \psi(p_s, P_c) \qquad (A\text{-}8)$$

The preceding eight equations contain the following eight unknowns u_w, u_s, p_w, p_s, S_s, S_s, T and u_h.

This analysis is restricted to steady-state fluid and heat flow. Thus, all derivations with respect to time are zero, and equation A3 can be integrated to yield

$$\rho_w u_w + \rho_s u_s = c(z) \qquad (A\text{-}9)$$

where c(z) is the constant of integration with respect to time. It represents the mass rate of flow. Because no fluid mass enters or leaves the porous media, the mass of the water flowing downward is equal to the mass of the steam flowing upward, and the net mass flow is zero. Thus c(z) equals zero and

$$\rho_w u_w = -\rho_s u_s \qquad \text{(A-10)}$$

The following equation for $\rho_w u_w$ can be obtained by eliminating u_s, $\frac{\partial p_w}{\partial z}$ and $\frac{\partial p_s}{\partial z}$ from equations A-1, A-2 and A-7.

$$\rho_w u_w = \frac{g(\rho_w - \rho_s)}{\frac{1}{\rho_s \lambda_s} + \frac{1}{\rho_w \lambda_w}} + \frac{(h_s - h_w)\left(\frac{\partial P_c}{\partial S_s}\frac{\partial S_s}{\partial z} + \frac{\partial P_c}{\partial T}\frac{\partial T}{\partial z}\right)}{\frac{1}{\rho_s \lambda_s} + \frac{1}{\rho_w \lambda_w}} \qquad \text{(A-11)}$$

Eliminating $\rho_s u_s$ from equations A-6 and A-10 yields

$$u_h = \rho_w u_w (h_w - h_s) - k_h \frac{\partial T}{\partial z} \qquad \text{(A-12)}$$

Under steady-state conditions, u_h is a constant which is equal to the heat flow rate at the surface.

Combining equations A-11 and A-12 yields

$$u_h = \frac{g(\rho_w - \rho_s)(h_w - h_s)}{\frac{1}{\rho_w \lambda_w} + \frac{1}{\rho_s \lambda_s}} + \frac{(h_s - h_w)\left(\frac{\partial P_c}{\partial S_s}\frac{\partial S_s}{\partial z} + \frac{\partial P_c}{\partial T}\frac{\partial T}{\partial z}\right)}{\frac{1}{\rho_w \lambda_w} + \frac{1}{\rho_s \lambda_s}} - k_h \frac{\partial T}{\partial z} \qquad \text{(A-13)}$$

As is customary in exploratory calculations such as these, the effects of capillarity are neglected, and equations A-11 and A-13 reduce to

$$\rho_w u_w = \frac{g(\rho_w - \rho_s)}{\frac{1}{\rho_w \lambda_w} + \frac{1}{\rho_s \lambda_s}} \qquad \text{(A-14)}$$

and

$$u_h = \frac{g(\rho_w - \rho_s)(h_w - h_s)}{\frac{1}{\rho_w \lambda_w} + \frac{1}{\rho_s \lambda_s}} - k_h \frac{\partial T}{\partial z} \qquad \text{(A-15)}$$

Eliminating u_w and u_s from equations A-1, A-2 and A-10 yields

$$\frac{\partial p}{\partial z} = \frac{g\rho_w^2\lambda_w + g\rho_s^2\lambda_s}{\rho_w\lambda_w + \rho_s\lambda_s} \qquad \text{(A-16)}$$

From equation A-8 (neglecting capillarity),

$$\frac{\partial T}{\partial z} = \frac{d\psi}{dp}\frac{\partial p}{\partial z} \qquad \text{(A-17)}$$

Eliminating $\frac{\partial T}{\partial z}$ and $\frac{\partial p}{\partial z}$ from equations A-13, A-16 and A-17 and converting to nondimensional form yields

$$AG_v + BG_d = 1 \qquad \text{(A-18)}$$

where

$$A = \frac{-k\ h_{wo}\ g\rho_{wo}^2}{u_h\ \mu_{wo}}$$

$$B = -\frac{g\rho_{wo}\ k_h}{u_h}\left(\frac{d\psi}{dp}\right)_o$$

$$G_v = \frac{\frac{\mu_{wo}}{k}\left(\frac{\rho_w - \rho_s}{\rho_{wo}}\right)}{\frac{\rho_{wo}}{\rho_w\lambda_w} + \frac{\rho_{wo}}{\rho_s\lambda_s}}$$

$$G_d = \frac{\left(\frac{d\psi}{dp}\right)\left(\frac{\rho_w^2}{\rho_{wo}}\lambda_w + \frac{\rho_s^2}{\rho_{wo}}\lambda_s\right)}{\left(\frac{d\psi}{dp}\right)_o(\rho_w\lambda_w + \rho_s\lambda_s)}$$

where ρ_{wo}, μ_{wo}, h_{wo} and $\left(\frac{d\psi}{dp}\right)_o$ correspond to boiling conditions at atmospheric pressure.

APPENDIX B

NOMENCLATURE

A, B = nondimensional coefficients (see equation A-18)

$c(z)$ = constant of integration with respect to time (see equations following equation A-9)

G_d, G_v = variable parts of fractional conductive and convective heat flow (see equation A-18)

g = gravitation constant

h = enthalpy

k_h = thermal conductivity

k, k_{rs}, k_{rw} = single phase permeability, relative permeabilities to steam and hot water respectively.

P_c = capillary pressure

p = fluid pressure

S = saturation

S_{s1}, S_{s2} = solutions of equation (1) (see Figure 4)

T = temperature

t = time

u = velocity as given by Darcy's law

u_h = heat flow rate

z = depth

λ = fluid mobility = $\frac{k\ k_r}{\mu}$

μ = viscosity

ϕ = porosity

ρ = density

ψ = boiling curve temperature expressed as a function of fluid pressure (Eq. A-8)

Subscripts

r = rock

s = steam

w = water

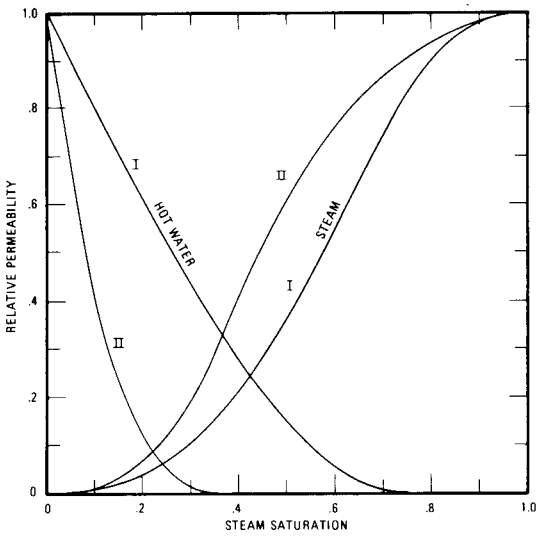

FIGURE 1
STEAM AND HOT WATER RELATIVE PERMEABILITY CURVES USED IN THE CALCULATIONS.

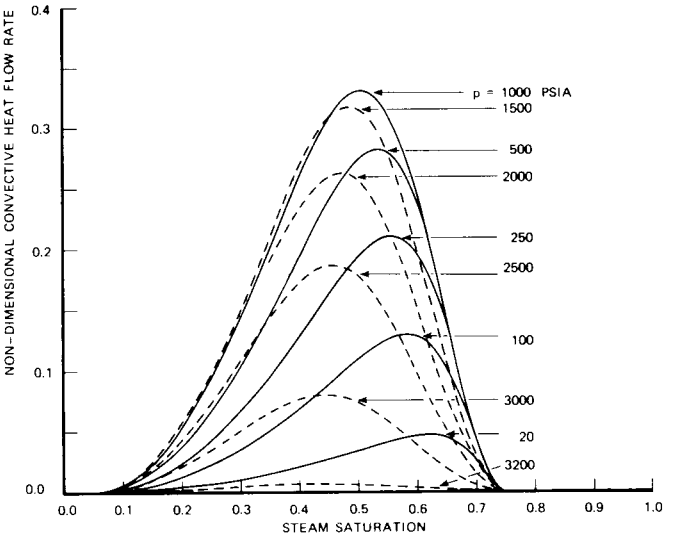

FIGURE 2
THE VARIATION OF THE NON-DIMENSIONAL CONNECTIVE HEAT FLOW RATE, G_v, WITH STEAM SATURATION, S_t, FOR VARIOUS VALUES OF FLUID PRESSURE FOR TYPE I RELATIVE PERMEABILITY CURVES.

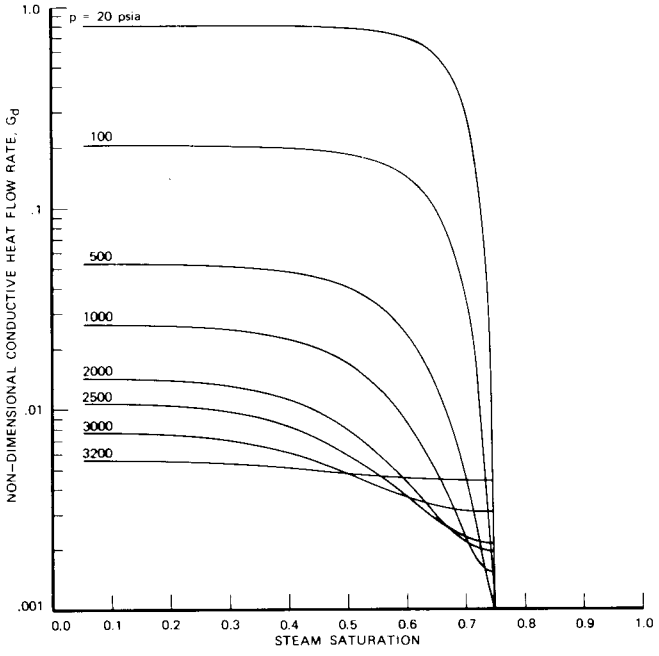

FIGURE 3
THE VARIATION OF THE NON-DIMENSIONAL CONDUCTIVE HEAT FLOW RATE, G_d, WITH STEAM SATURATION FOR VARIOUS VALUES OF FLUID PRESSURE FOR TYPE I RELATIVE PERMEABILITY CURVES.

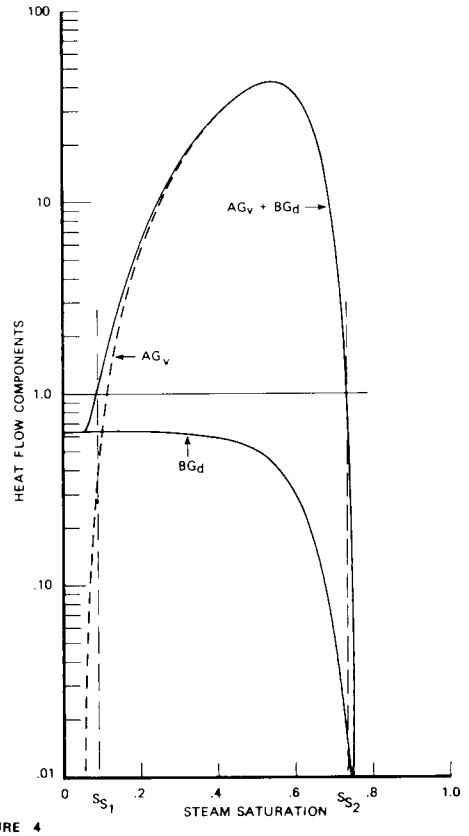

FIGURE 4
THE VARIATIONS OF THE FACTIONAL CONVECTIVE AND CONDUCTIVE HEAT FLOW RATES, AG_v AND BG_d, AND $AG_v + BG_d$ WITH STEAM SATURATION. THE SATURATIONS S_{s1} AND S_{s2} ARE THE TWO SOLUTIONS OF EQUATION (1) FOR TYPE I RELATIVE PERMEABILITY CURVES.

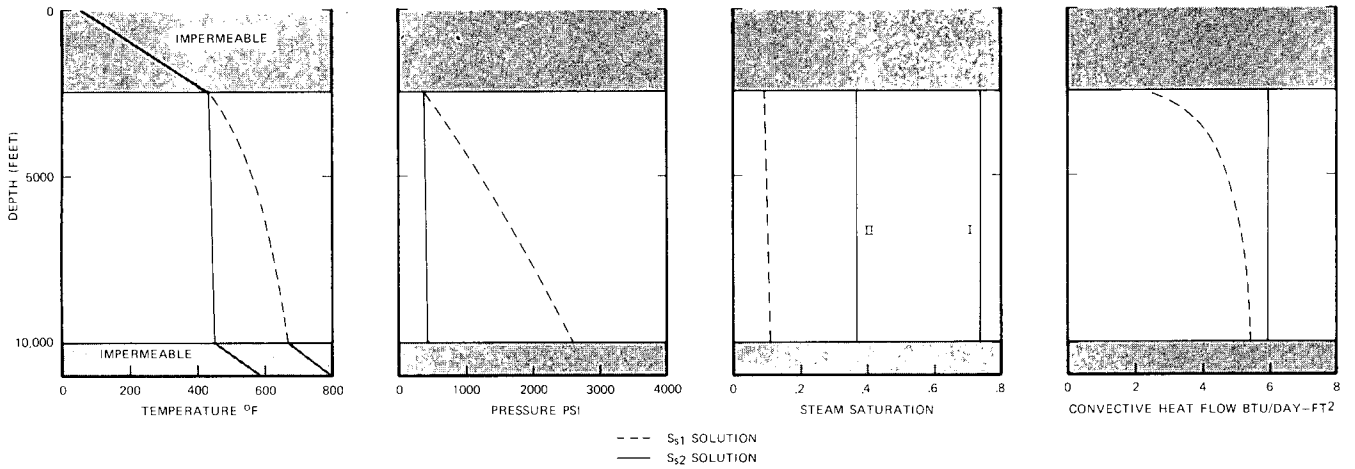

FIGURE 5

CALCULATED RESULTS FOR THE TWO SATURATION SOLUTIONS, S_{s1}, S_{s2}, BEGINNING AT THE TOP OF THE RESERVOIR FOR k = .01 DARCYS, k_h = 40 BTU/DAY–FT–°F, AND u_h = –6 BTU/DAY–FT^2. THE S_{s1} SOLUTION APPROXIMATES HOT WATER COLUMN CONDITIONS AND THE S_{s2} SOLUTION APPROXIMATES STEAM COLUMN CONDITIONS. RELATIVE PERMEABILITY TYPES ARE DENOTED BY I AND II.

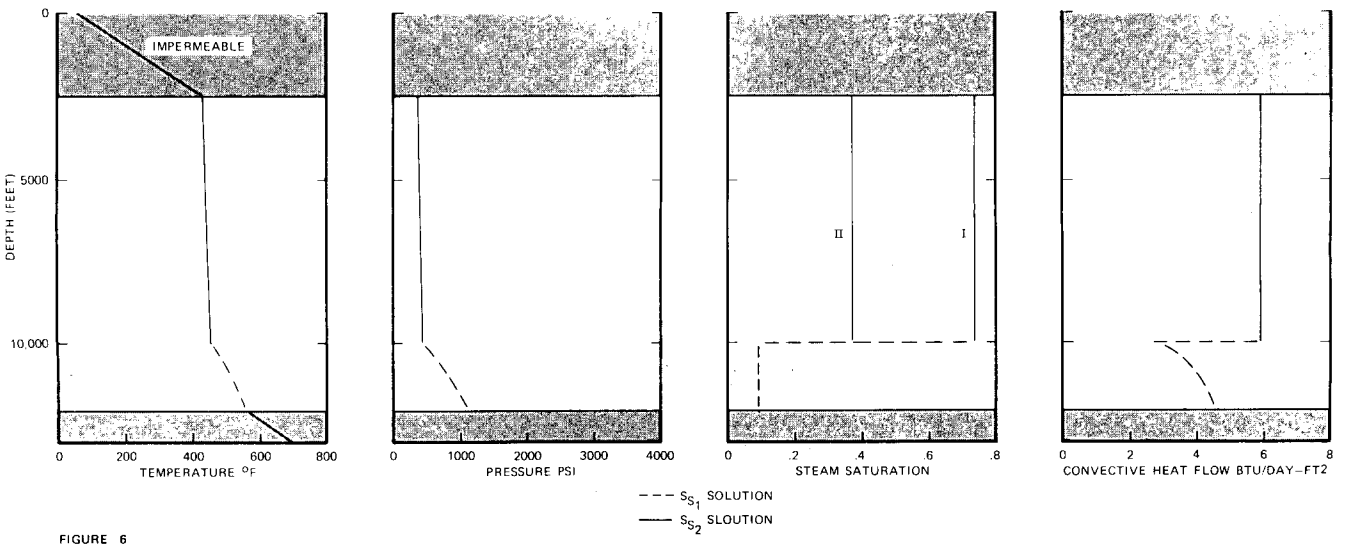

FIGURE 6

CALCULATED RESULTS FOR A HOT WATER–STEAM INTERFACE AT 10,000 FEET FOR SAME PARAMETERS USED IN FIGURE 5. THE S_{s2} SOLUTION APPLIES FROM 2500 TO 10,000 FEET AND THE S_{s1} SOLUTION APPLIES FROM 10,000 TO 12,000 FEET. RELATIVE PERMEABILITY TYPES ARE DENOTED BY I AND II.

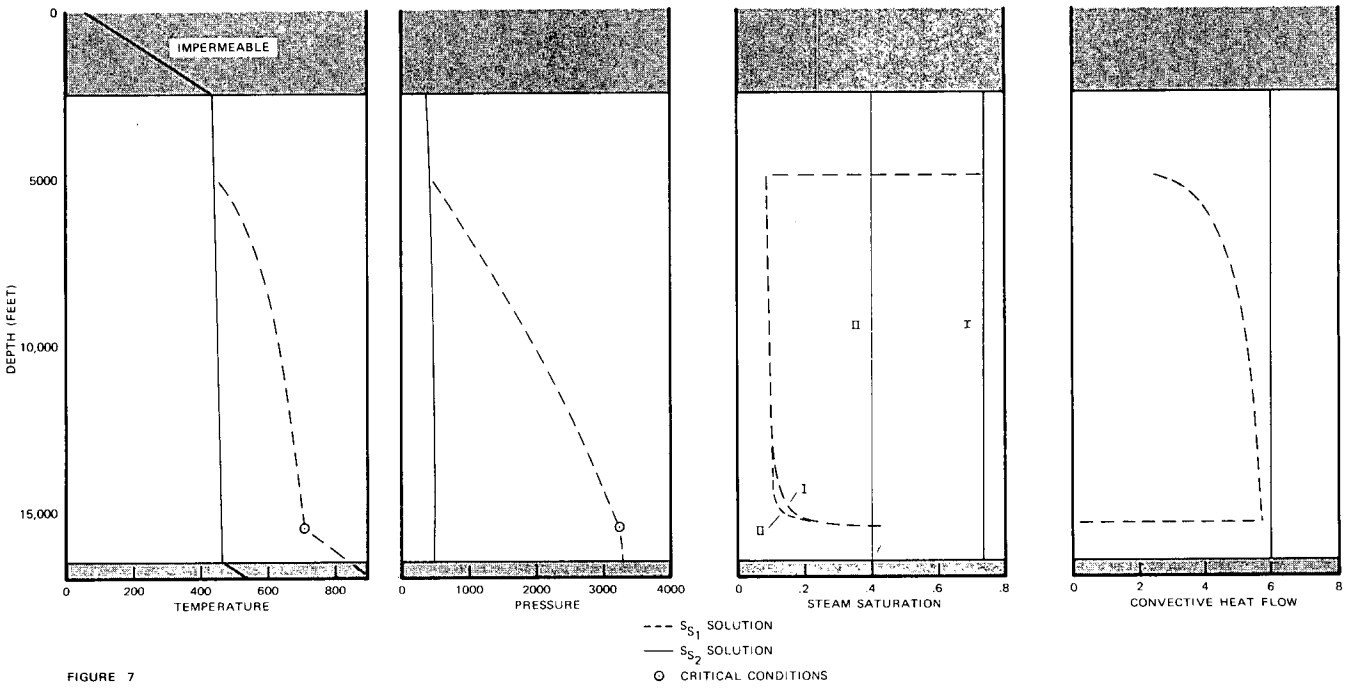

FIGURE 7

CALCULATED RESULTS WITH AND WITHOUT A INTERFACE AT 5000' FOR THE SAME PARAMETERS THOSE USED IN FIGURE 5. RELATIVE PERMEABILITY TYPES ARE DENOTED BY I AND II.

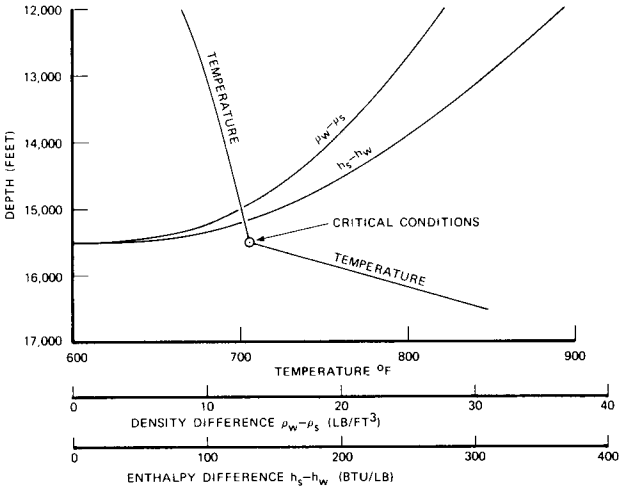

FIGURE 8

THE VARIATIONS OF THE DENSITY AND ENTHALPY DIFFERENCES NEAR CRITICAL CONDITIONS FOR THE S_{s1} SOLUTION PRESENTED IN FIGURE 7.